ELSEVIER

Physics of the Earth and Planetary Interiors 127 (2001) 145–163

PHYSICS OF THE EARTH AND PLANETARY INTERIORS

www.elsevier.com/locate/pepi

Seismological constraints on the mechanism of deep earthquakes: temperature dependence of deep earthquake source properties

Douglas A. Wiens*

Department of Earth and Planetary Sciences, Washington University, 1 Brookings Dr., St. Louis, MO 63130, USA

Received 25 May 2000; accepted 26 November 2000

Abstract

Seismological observations are of vital importance for understanding the mechanism of deep earthquakes. Most of the seismological observables for earthquakes deeper than 300 km are similar to shallow earthquakes. Deep earthquakes clearly represent shear failure on a planar surface as shown by their double couple mechanisms. Deep earthquake aftershock sequences show temporal decay rates and magnitude–frequency relations (*b*-values) that are similar to shallow earthquakes, with the aftershocks occurring preferentially along the mainshock fault planes. In addition, deep earthquake rupture velocities are similar to those of shallow earthquakes. However, there are also some observations that are clearly distinctive relative to shallow earthquakes. Stress drops of deep earthquakes show a large variation but are larger, on average, than shallow earthquakes. Different deep seismic zones show very different *b*-values, in contrast to shallow earthquakes, which show similar *b*-values worldwide. In addition, deep earthquakes show fewer aftershocks than shallow earthquakes.

A variety of observations suggest that deep earthquakes are highly sensitive to the temperature of the slab. Both deep earthquake *b*-values and the rate of deep earthquake aftershock occurrence are inversely correlated with the temperature of the deep slabs, suggesting that these factors are temperature-controlled to an extent much greater than with shallow earthquakes. Large deep earthquakes in warm slabs show slower rupture velocities, larger stress drops, and lower seismic efficiencies than similar earthquakes in cold slabs. The width of deep seismic zones is also probably temperature controlled, but deep earthquake rupture can propagate outside the normal limits of Benioff zone seismicity. Simple thermal models for the Tonga slab near the 1994 deep earthquake suggest that the temperature at the rupture termination point was at least 200°C warmer than the temperature that limits smaller earthquakes in the slab.

These observations can be used to evaluate physical models for deep earthquakes, including brittle slip along fluid-weakened faults, transformational faulting, and thermal (and perhaps melt lubricated) shear instabilities. It is difficult to explain the large fault widths of some deep earthquakes using a fluid weakening model, since hydrated materials are expected in only a narrow depth zone at the top of the slab, and the fault planes do not have the expected orientations for reactivated faults. The lateral extent of the largest deep earthquakes cast doubt on the transformational faulting model, in which events should be confined within a narrow metastable wedge. Seismological studies have also failed to find evidence for the existence of metastable olivine in slabs. The temperature dependence of deep earthquakes argues in favor of a temperature-activated phenomenon, such as thermal shear instabilities and perhaps fault zone melting.

Keywords: Seismology; Deep earthquake; Magnitude–frequency relation

1. Introduction

The mechanism and tectonic interpretation of deep earthquakes remains one of the major questions in

* Tel.: +1-314-935-6517; fax: +1-314-935-7361.
E-mail address: doug@mantle.wustl.edu (D.A. Wiens).

0031-9201/01/$ – see front matter
PII: S0031-9201(01)00225-4

seismology and rock mechanics. It has long been recognized that the occurrence of deep earthquakes is problematic, since brittle failure should be prohibited by confining pressure at great depth (Leith and Sharpe, 1936). In addition, deep earthquakes show interesting differences with shallow brittle faulting earthquakes, including much lower aftershock production rates (Page, 1968; Frohlich, 1989; Wiens et al., 1997), a dependence of source duration and rise time on earthquake depth (Houston and Williams, 1991; Vidale and Houston, 1993; Houston et al., 1998), and a dependence of magnitude–frequency relations and aftershock productivity on slab temperature (Wiens and Gilbert, 1996).

In recent years, a variety of mechanisms have been proposed to explain deep earthquake faulting. High fluid pressure resulting from possible dehydration reactions have been proposed to reduce the effective confining pressure and allow movement on pre-existing faults (Meade and Jeanloz, 1991; Silver et al., 1995). Transformational faulting (anticracks), in which the transformation from metastable α-olivine to a denser β-phase is accompanied by localization of strain into thin shear zones, has been suggested based on laboratory experiments (Kirby, 1987; Green and Burnley, 1989; Burnley et al., 1991; Kirby et al., 1991, 1996b; Green and Houston, 1995; Marone and Liu, 1997). It has also been proposed that shear failure propagates as ductile faulting or plastic instabilities (Ogawa, 1987; Hobbs and Ord, 1988) rather than as brittle failure, or that rupture propagation is facilitated by melt production at the crack tip (Kanamori et al., 1998). All of these proposals involve large extrapolation from laboratory experiments or calculations to the depths and scale lengths of deep earthquakes, and therefore remain speculative.

The major constraints on the mechanism and interpretation of deep earthquakes are provided by seismological observations, in combination with mineral physics experiments and geodynamic calculations. In this paper, I review the basic seismological observations concerning deep earthquakes, and discuss their implications for our understanding of the mechanism of deep earthquakes and the geodynamics of subducting slabs. The focus of this paper will be earthquakes deeper than 300 km; intermediate depth earthquakes (70–300 km) show many characteristics in common with deep earthquakes but it is unclear whether they result from similar processes (Meade and Jeanloz, 1991; Abers, 1996; Kirby et al., 1996a).

2. Comparison of deep and shallow earthquakes

Our knowledge of earthquakes is based primarily on observations of shallow earthquakes, which can be intensively studied using close-in seismological and geodetic instrumentation and direct field observations. Since good models have been developed for shallow earthquakes based on these observations, I will first review the characteristics of deep earthquakes in comparison with shallow earthquakes before discussing specific models of deep earthquake occurrence.

2.1. Seismic source geometry

The seismic source parameters of deep earthquakes are generally indistinguishable from the source parameters of typical shallow earthquakes. In the past, it was thought that deep earthquake sources might deviate systematically from the double couple source that is indicative of shear movement along a plane, and which is observed for nearly all shallow earthquakes. Dziewonski and Gilbert (1974) proposed that some deep earthquakes showed significant isotropic components, indicating a volume change. Randall and Knopoff (1970) proposed that deep earthquakes showed a significant compensated linear vector dipole (CLVD) component, which can be visualized as motion away from (or toward) the source along a polar axis, with a corresponding opposite motion along an equatorial band (Frohlich, 1994). These anomalous seismic sources were thought to be indicative of the causative mechanism of deep earthquakes, such as phase changes.

It is now clear that deep earthquakes generally show negligible isotropic components (Fig. 1a) (Hara et al., 1996; Kawakatsu, 1996; Russakoff et al., 1997). Deep earthquakes do show significant CLVD components, but in approximately the same proportions observed for shallow earthquakes (Fig. 1b) (Kuge and Kawakatsu, 1993). The CLVD components could be due to the effects of compound rupture, where slip occurs along several faults of different orientation during the event (Kuge and Kawakatsu, 1993; Frohlich, 1994). These results indicate that deep earthquakes

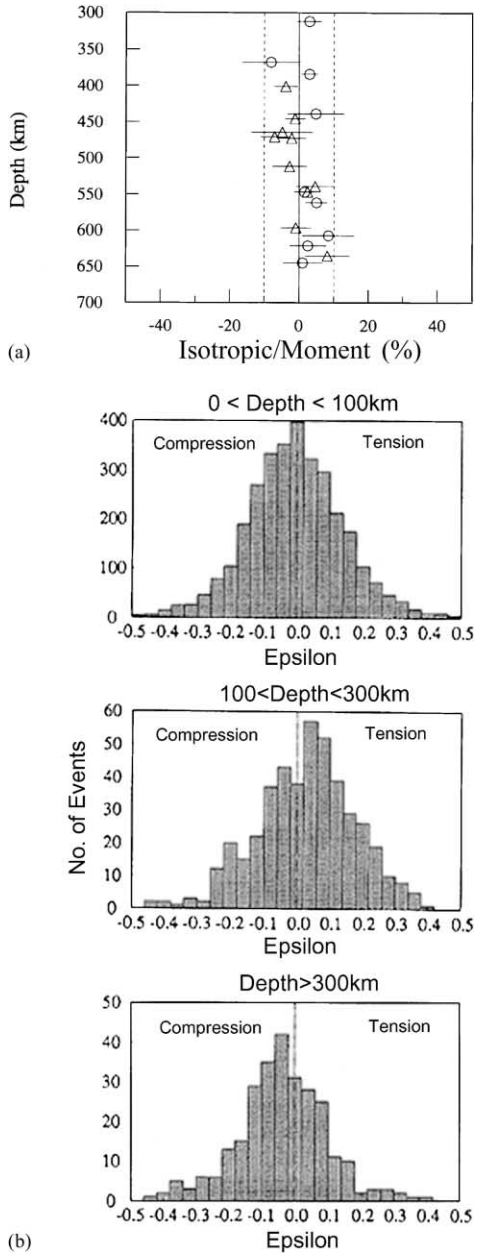

Fig. 1. (a) The isotropic component (%) of the moment tensor for 19 deep earthquakes, with earthquake depth plotted along the vertical axis (Kawakatsu, 1996). None of the earthquakes show a resolvable isotropic (volumetric) component. (b) Histograms showing the deviatoric non-double couple component for Harvard centroid moment tensor solutions (Kuge and Kawakatsu, 1993). Epsilon is 0 for a pure double couple and ±0.5 for a pure CLVD source. There is no significant increase in non-double couple component with depth.

must represent largely shear motion along a planar surface; any volumetric component resulting from a phase transformation must be much smaller than the shear slip.

2.2. Rupture characteristics

Seismological source studies allow seismologists to determine a variety of rupture characteristics for deep earthquakes, including average rupture velocity, static stress drop, and maximum seismic efficiency. The static stress drop represents the difference between the stress on the fault before and after the earthquake, and is proportional to the ratio of the fault displacement to the fault width. The maximum seismic efficiency is the ratio of the energy radiated elastically to the total energy release (Kikuchi, 1992). The difference between radiated and total energy is lost to friction along the fault. Due to the absence of near-field geodetic and strong ground motion measurements, these parameters are more uncertain for deep earthquakes than for well-studied shallow events. The uncertainties for deep events are a function of the spatial and temporal separation of the rupture events, so the rupture characteristics are better resolved for the larger events. For the largest deep earthquakes, the uncertainty in stress drop and seismic efficiency is probably a factor of 2, whereas the average rupture velocity can be somewhat better resolved.

Table 1 presents a synthesis of the best estimates of the rupture parameters of all deep earthquakes of $M_w = 7.5$ and greater since 1960. Details about how these parameters were determined are given in Appendix A, along with Table 2 listing the actual derived parameters from individual prior studies.

Deep earthquakes show a wide variety of rupture velocities, stress drops, and seismic efficiencies. Average rupture velocities range from 1.7 to 4.1 km/s. These rupture velocities are indistinguishable from rupture velocities for large shallow earthquakes. For example, in the tabulation of Geller (1976), rupture velocities range from 1.4 to 4.0 km/s, with most in the range of 2–3 km/s. As rupture velocity is thought to be limited by the shear wave velocity (Johnson and Scholz, 1976), it may be more appropriate to compare the ratio of rupture velocity to shear velocity. Since shear velocity is higher for deep earthquakes, this ratio is lower for the deep events. However, any differences

Table 1
Source parameters of the largest deep earthquakes

Date	Location	M_w	Depth (km)	Thermal parameters (km)	Aftershocks $m_b \geq 4.5$	Mo (10^{20} Nm)	Radiated energy (10^{14} J)	Rupture velocity (km/s)	Stress drop (MPa)	Rupture diameter (km)	Duration (s)	Scaled duration[a] (s)	Maximum efficiency
9 June 94	Bolivia	8.3	637	1800	3	26	290	1.7	44	60×45	40	40	0.061
31 July 70	Colombia	8.0	651	1800	0	14	23	2.0	38	100×20	60	72	0.010
17 June 96	Flores Sea	7.8	587	9400	14	7.3	180	4.0	16	90×25	23	35	0.370
29 September 73	Japan Sea	7.7	575	5600	0	5	10	3.3	10	60×40	24	41	0.046
15 August 63	Bolivia	7.7	543	1800	0	3.9	12	2.0	22	60×20	34	64	0.033
9 November 63	Brazil	7.6	600	1800	2	3.5	16	3.0	27	40×25	20	39	0.041
9 March 94	Tonga-Fiji	7.6	564	11800	29	3.1	24	4.1	15	45×30	14	28	0.120

[a] Duration of source time function divided by $M_0^{1/3}$ to remove the effect of event size and scaled to the duration of the Bolivia event.

are still minor compared to variations within both the shallow earthquake and deep earthquake populations.

Static stress drops for the deep events range from 10 to 44 MPa, somewhat greater than the stress drops of 3–10 MPa typically found for shallow events (Kanamori and Anderson, 1975). Thus, deep earthquakes show greater static stress drops than shallow earthquakes on average, as proposed by several previous studies (Chung and Kanamori, 1980; Fukao and Kikuchi, 1987). However, some deep earthquakes, such as the 1973 Japan Sea, 1994 Tonga–Fiji, and 1996 Flores Sea events show stress drops lower than 20 MPa and thus within the range shown by shallow earthquakes. Higher static stress drops can also explain previous suggestions that deep earthquakes show smaller rise times (Houston and Williams, 1991) and shorter source durations (Vidale and Houston, 1993). It should be noted that some reports of uniform stress drop with depth (Houston and Williams, 1991) are based on the Orowan stress drop (Vassiliou and Kanamori, 1982), a dynamic stress drop (equal to the static stress drop times the seismic efficiency) that assumes conditions unlikely to be fulfilled for deep earthquakes.

Deep earthquakes also show a wide range of maximum seismic efficiencies, ranging from 0.01 to 0.31. Thus, some deep earthquakes are quite efficient at converting available energy into seismic radiation, whereas other events loose more energy to friction and other dissipative processes. The seismic efficiencies of shallow earthquakes are not well constrained, but range from 0.04 to 0.22 in the study of Kikuchi (1992), and from 0.1 to 1.0, if the average apparent stresses for various tectonic settings given in Choy and Boatwright (1995) are converted to maximum seismic efficiencies. So, the seismic efficiencies of most deep earthquakes fall within the range of shallow earthquakes, but there is evidence that some deep earthquakes show unusually low seismic efficiencies, suggesting a more dissipative process (Kanamori et al., 1998).

2.3. Aftershock sequences

The smaller number of aftershocks observed for deep earthquakes may be the most obvious difference between shallow and deep earthquakes, and has been discussed by many investigators (Page, 1968; Kagan and Knopoff, 1980; Frohlich, 1987). Until recently, little was known about deep earthquake aftershocks, since significant deep aftershock sequences were unknown. However, the identification of several substantial deep aftershock sequences (Wiens et al., 1994; Myers et al., 1995; Wiens, 1998; Wu and Chen, 1999) has recently lead to a better understanding of deep earthquake aftershock characteristics.

Deep earthquake aftershock sequences generally show aftershock productivity rates of one to three orders of magnitude less than shallow earthquakes of equivalent size. A survey of aftershock sequences from moderate-sized deep earthquakes in the Tonga subduction zone suggests that they show an order of magnitude less aftershock activity than sequences from similar-sized mainshocks in California (Wiens et al., 1997). The 9 March 1994 Tonga deep earthquake showed the strongest known deep aftershock sequence, with 144 aftershocks (Wiens et al., 1994; Wiens and McGuire, 2000). This sequence is equiv-

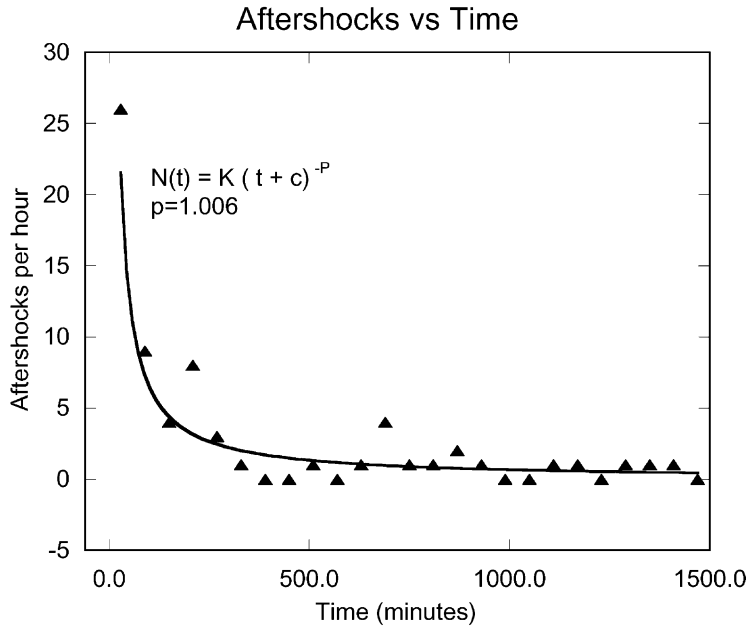

Fig. 2. Temporal decay of the aftershock occurrence rate for aftershocks with $m_b \geq 3.8$ during the first day following the 9 March 1994 Tonga deep earthquake. The line shows the fit obtained from a maximum likelihood analysis of the entire sequence.

alent to a rather weak aftershock sequence for a shallow earthquake of the same size. The stronger deep aftershock sequences generally show *b*-values and temporal decay rates that are similar to shallow earthquakes (Wiens et al., 1994; Nyffenegger and Frohlich, 2000; Wiens and McGuire, 2000). Fig. 2 shows that the temporal decay characteristics of the 9 March 1994 Tonga earthquake are well fit by a power law decay with an exponent (*P*-value) of 1.0, which is identical to typical shallow earthquakes (Wiens and McGuire, 2000). The similarity of deep and shallow earthquake *P*-values may be significant, since prior studies of shallow earthquakes suggest that *P*-values are indicative of the physical characteristics of the source region (Kisslinger, 1996).

The aftershock productivity of deep earthquakes also shows a strong variation between different deep seismic zones (Wiens and Gilbert, 1996). Deep earthquakes in Tonga and the Marianas generally show relatively strong aftershock sequences, whereas deep earthquakes in the Japan, Kurile, and South American subduction zones show few aftershocks relative to their seismic moment. For example, the two largest deep earthquakes known have occurred in South America, and both show few aftershocks (the 1994 Bolivia event ($M_w = 8.3$) shows only three aftershocks with $m_b \geq 4.5$, and the 1970 Colombia event ($M_w = 8.0$) had no known aftershocks). In contrast, the 1994 Tonga event ($M_w = 7.6$) showed 29 aftershocks with $m_b \geq 4.5$, and even a much smaller event such as the 1995 Mariana deep earthquake ($M_w = 7.0$) showed nine aftershocks with $m_b \geq 4.5$ (Wu and Chen, 1999). The systematic variation in deep earthquake aftershock production as a function of source region (Wiens and Gilbert, 1996) seems unlike shallow earthquakes, where aftershock productivity has been characterized as a simple function of mainshock fault area (Yamanaka and Shimazaki, 1990).

Aftershocks of deep earthquakes appear to concentrate along the mainshock fault plane (Wiens et al., 1994), as do aftershocks of shallow earthquakes. For shallow earthquakes Kisslinger (1996), classifies aftershocks as class 1, located along the rupture zone of the mainshock, class 2, located along the mainshock fault but not within the rupture zone, and class 3, which may be located anywhere in the vicinity. The majority of shallow aftershocks are class 1, particularly if they occur within the first 24–48 hours after

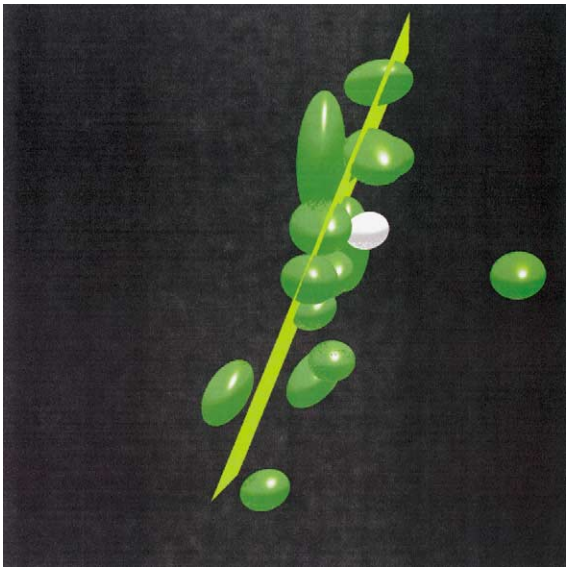

Fig. 3. Three-dimensional view of the best-located aftershocks of the 9 March 1994 Tonga deep earthquake. Ellipsoids denote the 95% confidence region of each earthquake location, with the white ellipsoid denoting the mainshock and the green ellipsoids denoting the best located aftershocks. The planar surface that best fits the aftershock locations is also shown; this plane is in good agreement with the mainshock focal mechanism.

the mainshock. Although past studies have suggested that deep earthquakes show aftershocks mostly of class 3 (Willemann and Frohlich, 1987), recent large deep earthquakes suggest that most aftershocks are concentrated near or along the mainshock rupture zone (classes 1 or 2). These deep earthquakes include the 1994 Tonga (Wiens et al., 1994; McGuire et al., 1997) and 1996 Flores Sea (Wiens, 1998; Tinker et al., 1998; Tibi et al., 1999) events. Fig. 3 illustrates the concentration of aftershocks along the fault plane of the 9 March 1994 Tonga deep earthquake. The 1994 Bolivia event shows fewer aftershocks along the mainshock fault plane, but the aftershocks are smaller and difficult to locate precisely (Myers et al., 1995).

The 1994 Tonga deep earthquake also showed an aftershock zone expansion pattern (Wiens and McGuire, 2000) similar to those observed for shallow earthquakes (Tajima and Kanamori, 1985). Aftershocks within the first 10 h were located mostly in regions of substantial mainshock moment release. This aftershock area expanded by about a factor of 2 over the next 24 h.

2.4. Magnitude–frequency relations

The slopes of deep earthquake magnitude–frequency relations (*b*-values) show a remarkable variation between different deep seismic zones (Giardini, 1988; Frohlich and Davis, 1993; Okal and Kirby, 1995; Wiens and Gilbert, 1996). Japan, the Kuriles, and South America are characterized by *b*-values (calculated from M_w) of 0.4–0.6 (Wiens and Gilbert, 1996),

(a)

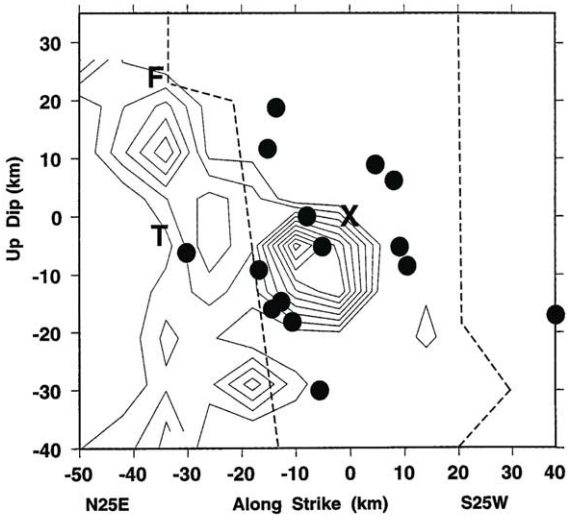

(b)

which is anomalously low relative to the typical values of 0.8–1.1 found for shallow events in all parts of the world (Frohlich and Davis, 1993). This indicates that large deep earthquakes are more numerous relative to small events than would be expected. In contrast, the *b*-value found for the Tonga deep subduction zone (1.28 ± 0.02) is higher than found for any shallow tectonic region, indicating a dearth of large earthquakes relative to the global average (Wiens and Gilbert, 1996). This behavior is different from shallow earthquakes, which show relatively constant *b*-values (Frohlich and Davis, 1993; Rundle, 1989), and where changes in *b*-values with increasing magnitude result from tectonic limitations on the width of the fault (Pacheco et al., 1992; Okal and Romanowicz, 1994).

3. Sensitivity of deep earthquakes to slab temperature

Some understanding that deep earthquakes are sensitive to the temperature of the slab has existed since early in the plate tectonics era. The maximum depth of intermediate and deep earthquakes is related to the temperature of the slab, as determined by the age of the subducting lithosphere and the convergence velocity (Molnar et al., 1979; Brodholt and Stein, 1988; Wortel and Vlaar, 1988). Recent evidence suggests that a variety of other deep earthquake statistical and rupture parameters are also a function of slab temperature. These observations may hold important clues about the mechanisms producing deep earthquakes.

3.1. Temperature limits on seismic nucleation and rupture

If the occurrence of deep earthquakes is temperature limited, slab thermal models suggest that the width of the seismically active zone should be controlled by the temperature range of faulting. Recent results show that the rupture and aftershock zone widths of the largest deep earthquakes are larger than the Benioff zone defined by smaller slab earthquakes (Wiens et al., 1994; McGuire et al., 1997). Fig. 4a shows the aftershock zone of the 9 March 1994 Tonga deep earthquake along with background seismicity. Two aftershocks occur 10–15 km beyond the limits of the Benioff zone as defined by small earthquakes. Fig. 4b shows a map of the slip distribution along the fault of the same earthquake, as determined by body waveform inversion, including regional broadband waveforms from the Southwest Pacific Seismic Experiment. This shows that the rupture also extended about 15 km beyond the nucleation limit of smaller slab earthquakes.

Slab thermal models allow some quantification of the different temperature limits for deep earthquake rupture and nucleation. Fig. 5 shows a thermal model of the Tonga subduction zone calculated using a finite difference method (Toksoz et al., 1973). Assuming that the center of the active seismic zone represents the coldest part of the slab, the features of the 1994 Tonga rupture can be mapped onto the thermal profiles. Unfortunately, uncertainties in many of the model parameters, such as the initial temperature structure of the Tonga slab, the subduction velocity, and the thermal conductivity (Hauck et al., 1999) are such that the absolute temperature structure is not

Fig. 4. (a) A cross-sectional view of the aftershock zone of the 9 March 1994 Tonga earthquake, viewed horizontally along the strike of the slab (N50°W) from the northwest (McGuire et al., 1997). Blue ellipsoids denote background seismicity, the white ellipsoid denotes the hypocenter of the 9 March 1994 Tonga event, the yellow ellipsoid denotes a foreshock, green ellipsoids denote aftershocks, and the red ellipsoid denotes the rupture termination point as determined from directivity analysis. The view is 90 km across, and earthquake depths range from 520 to 610 km. This figure shows that the background seismicity in this region forms an indistinct double seismic zone, and that the rupture propagated into the previously aseismic region. At least two aftershocks also initiated in the aseismic region. (b) A view of the seismic slip as a function of position along the fault plane of the 1994 Tonga deep earthquake, as determined by body waveform inversion of 47 P- and SH-phases (McGuire et al., 1997). The slip is shown with a contour interval of 0.5 m. The view is from the northwest, perpendicular to the fault plane, and is directly comparable with (a). The location of the edges of the background seismicity are plotted as dotted lines, the hypocenter is denoted as 'X', well-located aftershocks as dots, a foreshock is denoted as 'F', and the location of the end of the rupture as determined by the directivity analysis is plotted as 'T'. The rupture initiated in the interior of the previously seismically active zone and proceeded to the northeast, extending about 15–20 km beyond the edge of the previously active seismic zone (vertical dotted lines). Aftershocks are concentrated in the active slab core in regions of low seismic moment release adjacent to the first subevent.

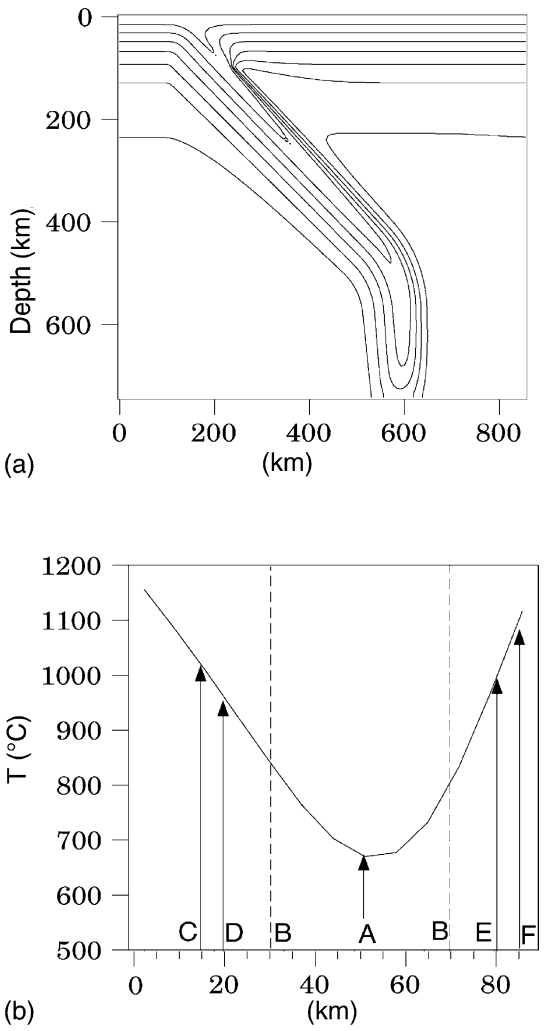

Fig. 5. (a) Thermal model of the Tonga slab, calculated with a finite difference method (Toksoz et al., 1973). The model was calculated assuming a convergence rate of 10 cm per year relative to the mantle. (b) Horizontal profile of temperatures through the slab model at the depth of the 1994 Tonga earthquake. Lateral locations of various features are shown, assuming that the seismic zone is centered on the coldest part of the slab. A denotes the epicenter location; B the edges of the background Wadati–Benioff zone seismicity, C the end of the rupture, D and E denote the outlying aftershocks to the northeast and southwest, respectively, and F denotes the position of the top of former oceanic crust in the thermal model. Although there is considerable uncertainty about the thermal model for the lower Tonga slab, the temperature difference of about 200°C between the limit of the background seismicity and the termination rupture is relatively robust. This suggests that deep earthquake ruptures can propagate through material that is at least 200°C warmer than the limiting temperatures for earthquake nucleation.

well constrained. However, by testing a wide variety of parameters for the thermal models, McGuire et al. (1997) determined that the temperature difference between the rupture termination point and the edge of the background seismicity is relatively robust, with differences of at least 200°C.

Thus, large earthquake ruptures can propagate through generally aseismic material until the rupture reaches temperatures that are 200–300°C warmer than the normal limiting temperature of deep seismicity in the slab. This suggests that slabs may be composed of a cold core, where seismic rupture initiates and small earthquakes occur, and a thermal "halo" of warmer material, which can sustain rupture, but no smaller earthquakes, and where aftershocks are generated only with difficulty during transient processes following large earthquakes.

3.2. Magnitude–frequency relations

The slope of the magnitude–frequency relation (*b*-value) is relatively constant within a given deep seismic zone but varies greatly between different zones (Giardini, 1988; Frohlich and Davis, 1993; Okal and Kirby, 1995; Wiens and McGuire, 1995). The variation in *b*-values between different deep seismic zones is related to the thermal properties of the subducting slabs, and seems to be a function of the slab thermal parameter (Wiens and Gilbert, 1996). The thermal parameter, the product of the slab vertical descent rate and the age of the subducting lithosphere, is a simple way of estimating the overall temperature structure of the deep slab. The use of the thermal parameter to compare temperatures at depth in the slab is justified theoretically if heating of the subducted lithosphere occurs by conduction and if the lithospheric temperature structure is given by a halfspace cooling model prior to subduction (Molnar et al., 1979). Larger thermal parameters correspond to cooler slab temperatures at depth. In this study, we use slab thermal parameters computed using the data given in Wiens and Gilbert (1996).

Fig. 6 shows *b*-values determined by a least squares fit to 1977–1995 M_w values for each deep seismic zone. The *b*-values show an obvious dependence on slab thermal parameter. Deep seismic zones in relatively warm slabs such as Peru–Chile show low *b*-values, indicating more large earthquakes relative

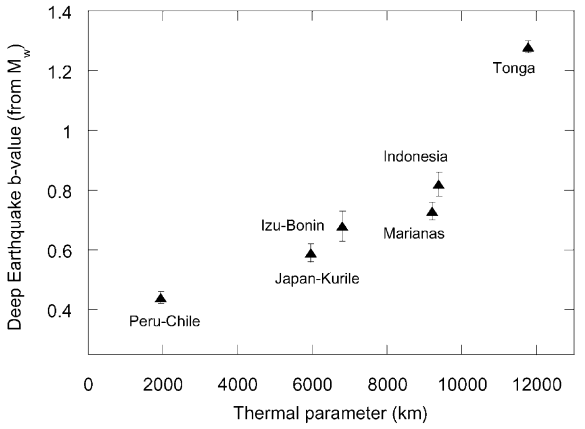

Fig. 6. The slope of the magnitude–frequency relation (*b*-value) for various deep seismic zones as a function of slab thermal parameter (Wiens and Gilbert, 1996). Cold deep seismic zones show a much higher *b*-value than warmer slabs, demonstrating that the statistical behavior of deep earthquakes is temperature dependent.

to small earthquakes. Deep earthquakes in colder slabs, such as Tonga, show much higher *b*-values, indicating more small earthquakes. This suggests that the statistics of deep earthquake occurrence is fundamentally temperature sensitive in a way that shallow earthquakes are not.

3.3. Aftershock productivity

Although there is substantial variability between events, the aftershock productivity of deep earthquakes when normalized by the mainshock size is correlated with the thermal parameter (Fig. 7) (Wiens and Gilbert, 1996). Fig. 7a tabulates aftershocks of all deep earthquakes 1958–1996 with $M_w \geq 7.0$ as a function of slab thermal parameter. Since the detection levels of small aftershocks varies with time and location, only aftershocks with $m_b \geq 4.5$ are tabulated. The number of aftershocks are normalized to the number expected for a $M_w = 8.3$ event, assuming that the number of aftershocks scales linearly with the seismic moment (Wiens and McGuire, 1995), as is observed in Japan and California (Yamanaka and Shimazaki, 1990). Fig. 7b tabulates all aftershocks of deep earthquakes with $M_w \geq 6.0$ from 1990 to 1996.

Both datasets suggest that the maximum number of aftershocks increases with the thermal parameter.

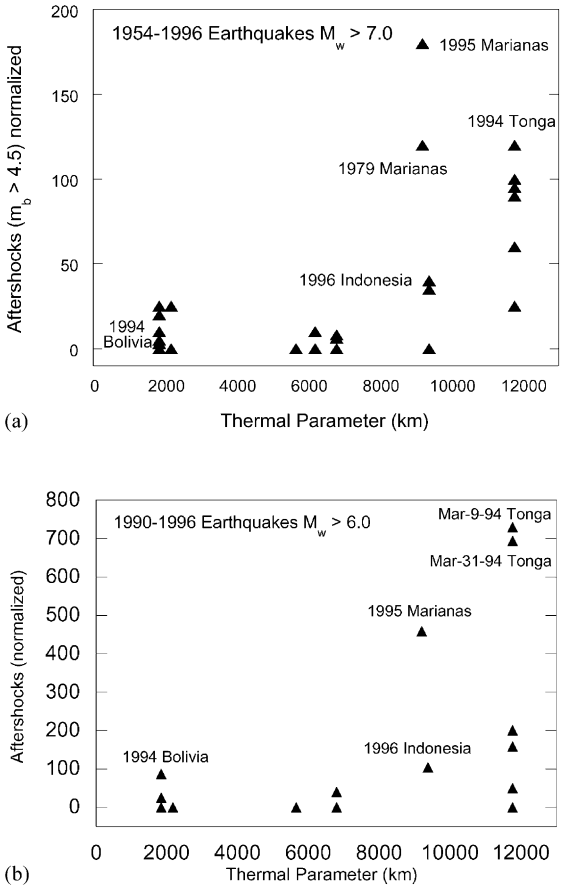

Fig. 7. (a) Number of normalized aftershocks ($m_b \geq 4.5$) for large 1958–1996 deep earthquakes as a function of subduction zone thermal parameter (Wiens and Gilbert, 1996). Larger thermal parameters correspond to cooler slabs. The number of aftershocks is normalized to correct for different mainshock sizes, assuming that the logarithm of the number of aftershocks is proportional to M_w, as observed for shallow earthquakes. (b) Total number of normalized aftershocks recorded for 1990–1996 deep earthquakes as a function of subduction-zone thermal parameter. Deep earthquakes in cold slabs show a much higher aftershock rate for both datasets.

Earthquakes with large numbers of aftershocks, such as the 1994 Tonga (Wiens and McGuire, 2000), the 1996 Flores Sea (Wiens, 1998), and 1995 Mariana (Wu and Chen, 1999) events are found only in relatively cold slabs with high thermal parameters. In contrast, earthquakes in warm slabs, such as the 1970 Colombia and 1994 Bolivia events, show few aftershocks relative to the mainshock moment. This observation is also correlated with the *b*-value of the deep seismic

zone, since zones showing low *b*-values also show few aftershocks, and vice-versa.

Deep earthquakes that produce many aftershocks are generally located in regions that show many smaller earthquakes, such as northern Tonga. Conversely, deep earthquakes producing few aftershocks are located in more aseismic regions, as measured by the number of small earthquakes. It is interesting to note that the four largest deep earthquakes since 1954 all occurred in regions showing essentially no smaller earthquakes at all, and all produced very few aftershocks (Wiens and McGuire, 1995). This phenomenon can be successfully described by the rate-and-state friction approach to aftershocks proposed by Dieterich (1994). In this model, a stress step such as an earthquake mainshock gives rise to a given seismicity rate change relative to the background rate. Therefore, mainshocks in highly seismic areas will produce many aftershocks, whereas similar sized mainshocks in largely aseismic areas will produce few aftershocks, in agreement with the deep earthquake data. However, this model does not explain the difference in aftershock rates between deep and shallow earthquakes, since some deep seismic zones show higher seismicity rates than shallow faults, yet produce one to three orders of magnitude fewer aftershocks.

Thus, the correlation of *b*-values and aftershock productivity with slab temperature may result from a similar phenomenon, the tendency for small earthquakes to be inhibited in warmer slabs. This phenomenon results in lower overall seismicity rates, low *b*-values, and fewer aftershocks in warmer slabs relative to cold slabs. Both the *b*-value and aftershock observations suggest that the statistics and occurrence of deep earthquakes are controlled by the slab temperature in a way that is fundamentally different from shallow earthquakes.

3.4. Earthquake rupture characteristics

Recent data indicates that the deep earthquake rupture characteristics may also be a function of the slab thermal structure (Table 1). Fig. 8 shows plots of rupture velocity, stress drop, scaled duration, and maximum seismic efficiency for the largest deep earthquakes (Table 1) as a function of slab thermal parameter. All of these parameters seem to show some dependence on the thermal parameter of the subduction zone. Earthquakes in warm slabs such as South America are characterized by slow rupture velocity, high stress drop, longer durations, and lower seismic efficiencies. Colder slabs, such as Tonga and Indonesia, are characterized by faster rupture velocities, lower stress drops, shorter durations, and higher seismic efficiencies. Since the low thermal parameter dataset is dominated by four large South American earthquakes, it could be that these differences arise through some other unique characteristic of the South American slab relative to western Pacific slabs, such as tectonics or composition. However, I choose to interpret these differences as resulting from thermal structure, in accord with the *b*-value and aftershock observations.

In general, the source parameters and aftershock characteristics of colder slabs are relatively similar to shallow earthquakes, whereas the observations from warmer slabs are quite different. For example, rupture velocities for the Tonga and Flores Sea events are about 75% of the shear velocity, which is similar to the average for shallow earthquakes (Geller, 1976). Conversely, rupture velocities for warmer slabs range from 30 to 55% of the shear velocity, or much lower than generally found for shallow earthquakes. The stress drops for deep earthquakes in cold slabs (10–16 MPa) are similar to the average stress drops for shallow intraplate earthquakes (∼10 MPa, Kanamori and Anderson, 1975), whereas stress drops for deep earthquakes in warm slabs are much greater (22–44 MPa). Similarly, deep earthquake efficiency, aftershock production, and *b*-values in cold slabs are more similar to shallow earthquakes than these parameters in warm slabs.

Overall, this survey of the source and aftershock parameters suggests that slab temperature has a major effect on the characteristics of deep earthquakes. This is an important clue in understanding the mechanism of deep earthquakes.

4. Proposed physical mechanisms of deep earthquakes

It has long been recognized that at depths greater than about 50 km, the stresses required for brittle faulting exceed any feasible strength of the material (Griggs and Handin, 1960; Leith and Sharpe, 1936). A variety of mechanisms to enable shear failure at

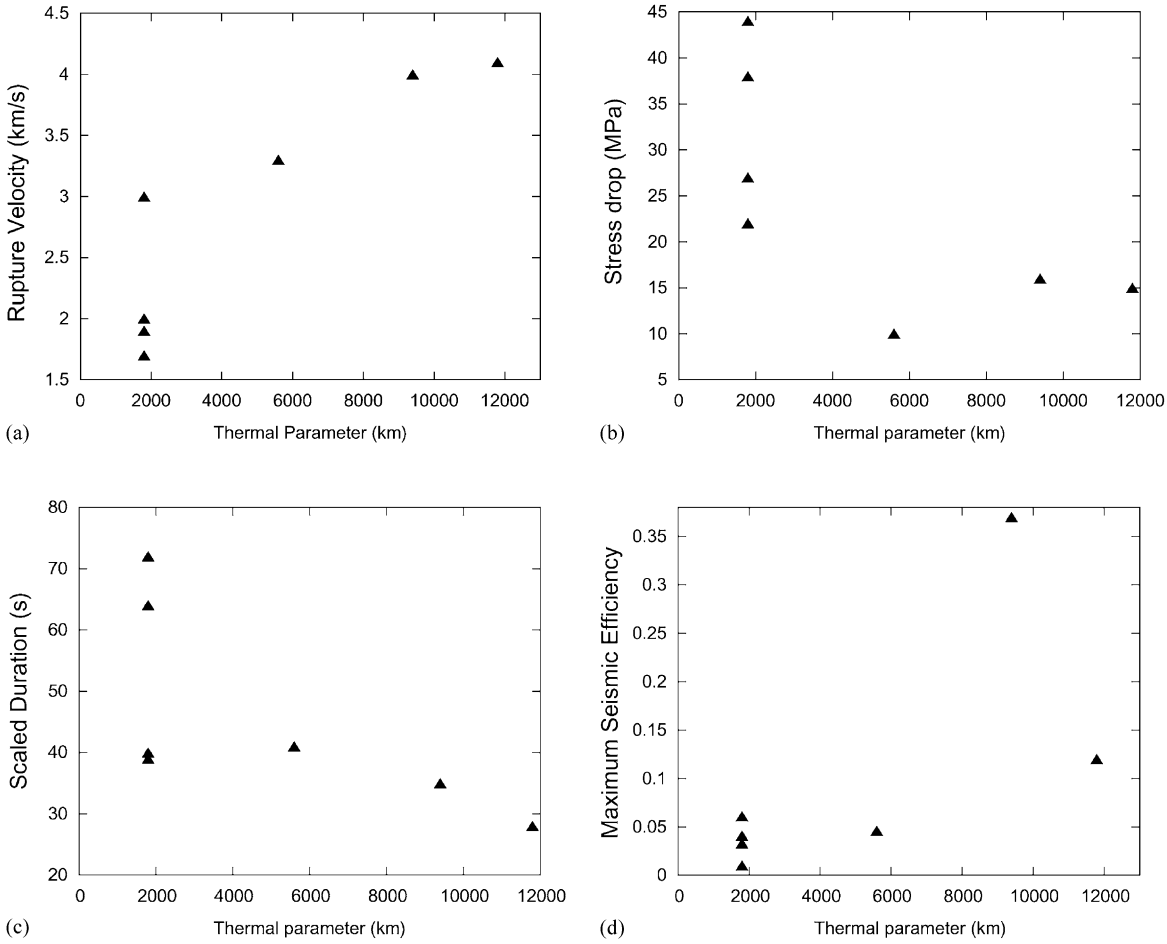

Fig. 8. (a) Average rupture velocity of large deep earthquakes as a function of slab thermal parameter, (b) static stress drop as a function of slab thermal parameter, (c) source time function duration, normalized by $M_o^{1/3}$ to correct for different seismic moments, as a function of slab thermal parameter and (d) maximum seismic efficiency as a function of thermal parameter. All source values are given in Table 1.

great depth have been proposed over the years, and are covered in several review papers (Frohlich, 1989; Green and Houston, 1995; Kirby et al., 1996b). Here, I briefly discuss the major proposed mechanisms and the evidence in light of recent research results.

4.1. Pore pressure and dehydration embrittlement

Earthquakes occurring under high confining pressures are commonly thought to result from high pore pressures, which reduce the effective normal stress on the fault (Hubbert and Rubey, 1959). It is unlikely that initial pore fluids can survive to great depths. However, water may be transported to depth as hydrous phases within a subducting slab (Thompson, 1992; Navrotsky and Bose, 1995; Bose and Navrotsky, 1998). Dehydration reactions may then liberate free fluids within regions of the slab containing hydrous minerals, thus leading to brittle failure at much smaller shear stresses (Raleigh and Paterson, 1965). Meade and Jeanloz (1991) documented acoustic emissions due to dehydration reactions in serpentinite at pressures of 2–9 GPa, and emissions resulting from metastable amorphization reactions at greater pressures.

Many studies have suggested that intermediate depth earthquakes (75–300 km depth) result from

dehydration embrittlement (Meade and Jeanloz, 1991; Green and Houston, 1995; Kirby et al., 1996a), since fluid phases are probably expelled from the slab at these depths (Tatsumi, 1989). However, the persistence of water and the existence of dehydration reactions at greater depth are less well established. Some deep dehydration reactions have negative ΔV (Bose and Navrotsky, 1998), such that the reaction produces a reduction in volume, which will generally prohibit dehydration embrittlement (Wong et al., 1997). Another difficulty is that hydrated phases are thought to exist largely in the upper few kilometers of the oceanic mantle (Meade and Jeanloz, 1991), whereas large deep earthquakes show much larger fault dimensions. This has lead to the proposal that shallow faults in the oceanic lithosphere represent weak zones along which water can circulate and form hydrated minerals. Deep earthquakes may thus represent dehydration embrittlement of these faults due to the concentration of hydrated minerals (Silver et al., 1995). However, the fault orientations of many deep earthquakes are not consistent with typical shallow fault orientations (McGuire et al., 1997; Jiao et al., 2000).

4.2. Transformational faulting

Early proposals linking deep earthquakes to phase transformations generally envisioned a process of sudden implosion caused by rapid transformation of a metastable lower-density phase (Bridgeman, 1945; Evison, 1967). As noted in the previous section, such volumetric mechanisms are inconsistent with the observation that deep earthquakes have double couple sources. However, Kirby (1987) suggested that deep earthquakes may result from shear dislocations associated with metastable phase transformations, and several high-pressure experimental studies soon found evidence of such phase transformations in both analogue and olivine systems (Green and Burnley, 1989; Green et al., 1990; Burnley et al., 1991).

The transformational faulting model suggests that the transition from α-olivine to β- or γ-phase is kinetically inhibited in the center of the coldest subducting slabs, resulting in a wedge of metastable α-olivine below the 410 km discontinuity (Sung and Burns, 1976; Rubie and Ross, 1994; Kirby et al., 1996b). Within this wedge, small lenses of transformed material (anticracks) form, and under a strong external stress field these lenses link up. The transformed material in the developing fault has little shear strength due to its fine grain size (Green and Burnley, 1989), and unlike brittle failure, faulting is not suppressed by confining pressure. The resulting failure results in the metastable transformation of the material in the fault zone to β- or γ-phase.

The transformational faulting model predicts that deep earthquakes should occur within a rather narrow, tapering metastable olivine wedge. The wedge should be largest for the coldest slabs, with thermal and kinetic modeling (Kirby et al., 1996b; Dassler and Yuen, 1996; Devaux et al., 1997; Hauck et al., 1999) as well as buoyancy considerations (Marton et al., 1999; Schmeling et al., 1999) suggesting widths of 5–25 km. In contrast, studies of the 1994 Tonga and Bolivia deep earthquakes suggest fault widths on the order of 40–50 km perpendicular to the slab (Wiens et al., 1994; Silver et al., 1995; McGuire et al., 1997). The total width of the aftershock zone of the 1994 Tonga event is about 65 km, demonstrating that earthquakes actually nucleate over a wide region. Both rupture propagation and aftershocks occurred outside the Benioff zone defined by smaller background seismicity, showing that the rupture zones and aftershocks of large deep events are not subject to the same spatial limitations that delineate small earthquakes in deep seismic zones.

There is also substantial doubt as to whether a metastable olivine wedge actually exists in deep slabs. Iidaka and Suetsugu (1992) found evidence of a metastable wedge in northern Izu–Bonin from seismic travel times. However, an experiment involving a better geometry of stations, including ocean bottom seismographs, in a colder slab (Tonga) yielded no conclusive evidence of a metastable wedge, and suggested that resolution of olivine metastability using travel times might be difficult (Koper et al., 1998). A finite difference modeling study of the Tonga slab suggested that a metastable wedge should produce prominent waveform distortion and later arriving phases due to guided energy propagating within the wedge; however, a search of the appropriate seismic records failed to find such effects (Koper and Wiens, 2000). Thus, there is little seismological evidence for olivine metastability in slabs, a primary requirement of the transformational faulting model.

4.3. Shear instabilities and melting

Griggs and Baker (1969), Ogawa (1987), and Karato (1997 and this issue) propose that deep earthquakes occur through a runaway thermal creep event along a shear zone. Rock creep induced by stress in a shear zone will produce heat, which conducts away very slowly. Since most creep processes are highly temperature sensitive, heating of the shear zone will lower the viscosity and promote a positive-feedback process in which further slip and heat is generated. Such a runaway creep event may result in melting along the fault zone. Hobbs and Ord (1988) suggested that below a critical temperature, mantle materials show strain rate softening behavior and may undergo catastrophic plastic shear. This model of plastic shear instabilities differs from the thermal shear instabilities in that the dominant control of shear zone development is strain rate hardening or softening rather than thermal effects.

Karato (this issue) suggests that the thermal runaway phenomenon would be favored in deep slabs due to rheological weakness caused by small grain size of the slab interior after the olivine to β-spinel transformation. Bina (1998) also notes that if olivine persists metastably below the depth for equilibrium transformation, latent heat release by the metastable transformation reaction will produce local superheating, which may favor the production of deep earthquakes by the thermal shear instability mechanism.

Kanamori et al. (1998) and Bouchon and Ihmle (1999) suggest that the slow rupture velocity, high stress drop, and low seismic efficiency indicate that runaway thermal creep and fault zone melting occurred during the 1994 Bolivia deep earthquake. They further show that the high stress drop would facilitate frictional heating, and that the low seismic efficiency might be indicative of significant energy dissipation due to heating and melt production during the faulting, leaving less energy available for seismic radiation.

Fig. 9 shows one conception of how the fault zone melting model might work, based on geologically observed fault zone melts (pseudo-tachylytes) (McKenzie and Brune, 1972; Spray, 1993; Obata and Karato, 1995). In this model, a zone of frictional melt production moves with the rupture front along the fault. Melt injection under high pressure may also occur ahead of the melt zone, perhaps facilitating crack propagation at the tip of the rupture. Melt production will reduce the friction along the fault, but this will then reduce the production of melt, such that an equilibrium between friction, melt production, and lubrication may allow the fault to propagate smoothly.

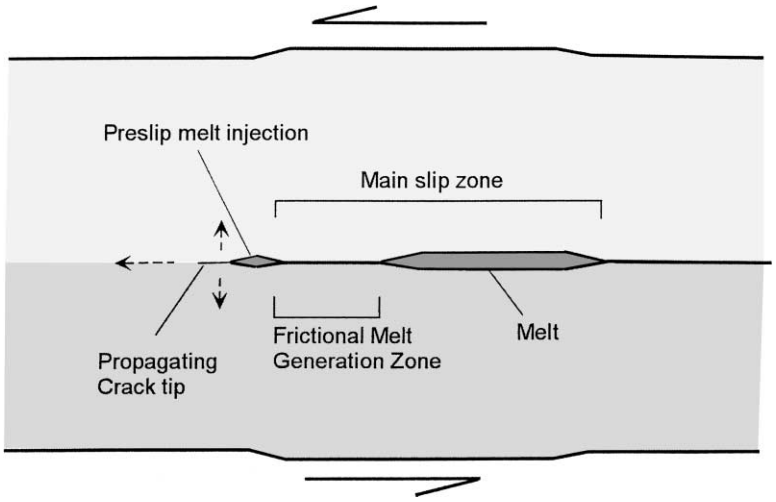

Fig. 9. Model for faulting with lubrication induced by frictional melting, originally developed to explain geological observations of pseudo-tachylytes in exhumed fault zones (after Spray, 1993). As the active slip zone moves along the fault, melting is induced by friction. If rupture propagation is slow, some melt may be injected ahead of the main slip zone, perhaps facilitating crack propagation.

Fig. 8 and Table 1 show that slow rupture, high stress drop, and low seismic efficiency seem to be characteristic of the largest deep earthquakes in warm slabs. According to the arguments presented in Kanamori et al. (1998), all of these earthquakes may involve fault zone melting, such that much of the elastic energy release is taken up in frictional heat production and melting, resulting in low seismic efficiency. In contrast, the earthquakes in colder slabs show faster rupture propagation, lower stress drop, and moderate seismic efficiency. In addition, deep earthquake magnitude–frequency relations and aftershock production show a dependence on slab temperature. Such a dependence of earthquake source properties on the temperature of the slab is to be expected if thermal shear instabilities and melting are the cause of deep earthquakes, since the precise mechanics of the thermal shear instability depend critically on the initial temperature of the rock.

One possibility, suggested by the different values of seismic efficiencies, is that deep earthquakes in warm slabs generally involve coseismic melting, whereas earthquakes in cold slabs represent thermal shear instabilities with little melting. The difference in rupture mechanics may result from the fact that the temperature in warmer slabs is closer to the melting point, and thus a highly dissipative thermal runaway involving melt is more readily attained. Magnitude–frequency relations would also be affected by slab temperature, since warm slabs would favor stress release through exceptionally large thermal runaway events, whereas colder slabs would show more typical *b*-values.

5. Conclusions

Deep earthquakes show many features that are similar to shallow earthquakes. Deep earthquakes represent shear failure on a planar surface, and show many similar statistical properties to shallow earthquakes, such as aftershock temporal decay characteristics. In addition, average rupture parameters are similar to shallow earthquakes, except that deep earthquakes tend to show higher stress drops.

However, some deep earthquake properties show a remarkable dependence on the source region, and vary systematically as a function of inferred slab thermal properties. Deep earthquake *b*-values and aftershock production rates are inversely correlated with slab temperature. In addition, deep earthquakes in warm slabs show slower rupture velocity, higher stress drop, and lower seismic efficiency relative to deep earthquakes in warm slabs. This dependence on temperature is unlike shallow brittle rupture.

Several models for the occurrence of deep earthquakes have been proposed. Dehydration embrittlement is a viable mechanism if it can be shown that hydrous minerals carry water to depths of 670 km. However, it is difficult to explain the large fault widths and orientations of some deep earthquakes, since hydrated phases are expected in only a narrow depth zone at the top of the slab, and the earthquakes do not have the expected orientations for reactivated shallow faults. In addition, dehydration mechanisms provide no explanation for the dependence of deep earthquake properties on slab temperature.

The transformational faulting model also fails to predict the large fault widths observed for deep earthquakes. Deep earthquakes rupture and aftershock nucleation occur throughout a wide region of the slab, in contrast to the narrow expected seismogenic zone within the metastable olivine wedge. There is little evidence that a large region of metastable olivine actually exists in slabs.

The shear instability model suggests that earthquake properties should be fundamentally sensitive to the temperature of the rock. In this way, it is qualitatively consistent with observations that magnitude–frequency relations, aftershocks, and rupture parameters vary systematically with slab temperature. Deep earthquakes in warm slabs show low seismic efficiencies, suggesting that they loose more energy to dissipative processes such as frictional heating and melting, perhaps as a result of the initially high temperatures of the rock in these regions. The thermal shear instability model is currently the most promising hypothesis concerning the physical mechanism of deep earthquakes, but further work on both observations of deep earthquake source parameters and the details of the shear instability mechanism are needed to evaluate this possibility.

Acknowledgements

I thank Patrick Shore, Jeffrey McGuire, Hersh Gilbert, and Keith Koper for use of figures and assis-

tance. I also thank Alan Rubin, Craig Bina, and Rob van der Hilst for helpful reviews, and Rigobert Tibi for comments on an earlier draft. Many of the results described here resulted from field studies, which used instruments provided by the PASSCAL program of Incorporated Research Institutions in Seismology (IRIS), and teleseismic data were obtained from the IRIS Data Management Center. This research was supported by the National Science Foundation under Grants EAR9418942 and EAR9805309.

Appendix A. Seismic source parameters of deep earthquakes

The seismic source parameters shown in table one were derived from numerous separate source studies performed by various investigators. Estimates of the source parameters obtained by these previous studies are tabulated in Table 2, and the references are listed in Table 3. Many of the parameters shown in the table are calculated somewhat differently by the various studies. Therefore, the following procedure was used to estimate the parameters given in Table 1.

Values for radiated energy, rupture velocity, rupture dimensions, and rupture duration were taken from the median of the values given by the previous studies. Greater weight was given to some of the studies. For example, in establishing the rupture dimension of the 1994 Bolivia earthquake, later studies (Antolik et al., 1996; Ihmle, 1998) make a strong case that the actual dimensions of the fault was larger than determined in some of the initial studies. Therefore, the fault dimensions chosen here (60 km ×

Table 2
Estimates of deep earthquake source parameters from previous studies

Date	Location	Radiated energy (10^{14} J)	Rupture velocity (km/s)	Stress drop (MPa)	Rupture diameter (km)	Rupture duration (s)	Maximum efficiency	Reference (Table 3)
9 June 94	Bolivia	520	1.0	110	40 × 40	40	0.036	KK
			1–2.6		50 × 30	40		S
			1.0	114	50 × 20	40		LG
			2–3	283	40 × 30	40		G
			1–2		50 × 30	45		C
		150	1.5–4	51	50 × 50	47	0.026	E
			1.7	150	60 × 40	40		A
			1.8	70	90 × 90	40		I
		250		71			0.02	WR
		320						U
31 July 70	Colombia	21	1.3	7	100 × 60	50	0.016	FK
		25	2	39	100 × 20	60	0.01	E
17 June 96	Flores Sea	290	4.0	21	95 × 20	23	0.45	T
			3.5	7–20	90 × 25	23		W
			4.5		75 × 30	29		TW
		58	2–4	16	105 × 20	20	0.05	G, WR
			>4.5	10	120 × 40	18		A
		180						U
29 September 73	Japan Sea	9.6	3.3	10	60 × 40	24	0.012	FK
15 August 63	Bolivia	17	3.3	4	80 × 50	37	0.043	FK
		7	2.0	17	60 × 20	34	0.033	E
9 November 63	Brazil	16	3.0	27	40 × 25	20	0.026	FK
9 March 94	Tonga-Fiji	11		7			0.25	WR
		37	5.0	25	40 × 20	14	0.15	T
			4.1	13	45 × 30	14		M
			3.0	14	60 × 20	17		LG
			4.0–5.0	26	40 × 30	12		G
		24						U

Table 3
References to deep earthquake source studies

Abbreviation	Reference
A	Antolik et al. (1996), (1999)
C	Chen (1995)
E	Estabrook and Bock (1995); Estabrook (1999)
FK	Fukao and Kikuchi (1987); Kikuchi (1992)
G	Goes and Ritsema (1995); Goes et al. (1997)
I	Ihmle (1998)
KK	Kikuchi and Kanamori (1994); Kanamori et al. (1998)
LG	Lundgren and Giardini (1995)
M	McGuire et al. (1997)
S	Silver et al. (1995)
T	Tibi et al. (1999)
TW	Tinker et al. (1998)
U	USGS (Preliminary determination of epicenters)
WR	Winslow and Ruff (1999)
W	Wiens (1998)

45 km) are somewhat larger than the median of the studies.

Because static stress drop calculations vary somewhat between different studies, and to ensure that the values given in Table 1 are self-consistent, stress drops were recalculated in this study using

$$\Delta\sigma = 2.4 \times \left(\frac{M_o}{A^{3/2}}\right)$$

This formula assumes that the rupture can be approximated as a circular fault, where A represents the fault area calculated from the dimensions given in Table 1, and M_o the seismic moment from the Harvard centroid moment tensor solutions (CMT) (Dziewonski et al., 1981). Thus, the static stress drop in Table 1 represents the average stress drop over the entire fault, and not the maximum stress drop associated with high moment release areas. Because the stress drop depends on the cube of the linear dimension of the fault, stress drop estimates have uncertainties of about a factor of 2.

The seismic efficiency is defined as the ratio of the radiated seismic energy to the total energy associated with the faulting event. It is difficult to estimate the actual seismic efficiency. However, with the assumption that the final stress after faulting is 0, it is possible to estimate the effective, or maximum seismic efficiency (Kikuchi, 1992) from

$$\eta = 2 \times \left(\frac{E_s}{M_o}\right)\left(\frac{\mu}{\Delta\sigma}\right)$$

where E_s is the radiated seismic energy and μ is the shear modulus. Assuming that the sliding friction is greater or equal to the final stress on the fault, this is the maximum possible seismic efficiency, since if the final stress on the fault is greater than 0, the seismic efficiency would be less than calculated with this method. Since the maximum seismic efficiency is calculated from the stress drop and the radiated seismic energy, both of which have considerable uncertainties, the derived values of are probably accurate to only a factor of 2.

References

Abers, G.A., 1996. Plate structure and the origin of double seismic zones. In: Bebout, G.E., Scholl, D.W., Kirby, S.H., Platt, J.P. (Eds.), Subduction Top to Bottom. Geophysics Monograph Series, AGU, Washington, DC, pp. 223–228.

Antolik, M., Dreger, D., Romanowicz, B., 1996. Finite fault source study of the great 1994 Bolivia deep earthquake. Geophys. Res. Lett. 23, 1589–1592.

Bina, C.R., 1998. A note on latent heat release from disequilibrium phase transformations and deep seismogenesis. Earth Planets Space 50, 1029–1034.

Bose, K., Navrotsky, A., 1998. Thermochemistry and phase equilibria of hydrous phases in the system MgO–SiO_2–H_2O: implications for volatile transport to the mantle (MgO–SiO_2–H_2O). J. Geophys. Res. 103, 9713–9720.

Bouchon, M., Ihmle, P.I., 1999. Stress drop and frictional heating during the 1994 Bolivia deep earthquake. Geophys. Res. Lett. 26 (23), 3521–3524.

Bridgeman, P.W., 1945. Polymorphic transitions and geologic phenomena. Am. J. Sci. 243A, 90–97.

Brodholt, J., Stein, S., 1988. Rheological control of Wadati–Benioff zone seismicity. Geophys. Res. Lett. 15, 1081–1084.

Burnley, P.C., Green, H.W., Prior, D.J., 1991. Faulting associated with the olivine to spinel transformation in Mg_2GeO_4 and its implications for deep focus earthquakes. J. Geophys. Res. 96, 425–443.

Choy, G.L., Boatwright, J.L., 1995. Global patterns of radiated seismic energy and apparent stress. J. Geophys. Res. 100, 18205–18228.

Chung, W.-Y., Kanamori, H., 1980. Variation of seismic source parameters and stress drops within a descending slab and its implications in plate mechanics. Phys. Earth Planet. Inter. 23, 134–159.

Dassler, R., Yuen, D.A., 1996. The metastable olivine wedge in fast subducting slabs: constraints from thermo-kinetic coupling. Earth Planet Sci. Lett. 137, 109–118.

Devaux, J.P., Schubert, G., Anderson, C., 1997. Formation of a metastable olivine wedge in a descending slab. J. Geophys. Res. 102, 24627–24638.

Dieterich, J., 1994. A constitutive law for rate of earthquake production and its application to earthquake clustering. J. Geophys. Res. 99, 2601–2618.

Dziewonski, A.M., Gilbert, F., 1974. Temporal variation of the seismic moment tensor and the evidence of precursive compression for two deep earthquakes. Nature 247, 185–188.

Dziewonski, A.M., Chou, T.-A., Woodhouse, J.H., 1981. Determination of earthquake source parameters from waveform data for studies of global and regional seismicity. J. Geophys. Res. 86, 2825–2852.

Evison, F.F., 1967. On the occurrence of volume change at the earthquake source. Bull. Seismol. Soc. Am. 57, 9–25.

Frohlich, C., 1987. Aftershocks and temporal clustering of deep earthquakes. J. Geophys. Res. 92, 13944–13956.

Frohlich, C., 1989. The nature of deep focus earthquakes. Ann. Rev. Earth Planet. Sci. 17, 227–254.

Frohlich, C., 1994. Earthquakes with non-double couple mechanisms. Science 264, 804–809.

Frohlich, C., Davis, S.D., 1993. Teleseismic *b*-values; or, much ado about 1.0. J. Geophys. Res. 98, 631–644.

Fukao, Y., Kikuchi, M., 1987. Source retrieval for mantle earthquakes by iterative deconvolution of long-period P-waves. Tectonophysics 144, 249–269.

Geller, R.J., 1976. Scaling relations for earthquake source parameters and magnitudes. Bull. Seismol. Soc. Am. 66, 1501–1523.

Giardini, D., 1988. Frequency distribution and quantification of deep earthquakes. J. Geophys. Res. 93, 2095–2105.

Green, H.W., Burnley, P.C., 1989. A new self-organizing mechanism for deep focus earthquakes. Nature 341, 733–737.

Green, H.W.I., Houston, H., 1995. The mechanics of deep earthquakes. Ann. Rev. Earth Planet. Sci. 24, 169–213.

Green, H.W., Young, T.E., Walker, D., Scholz, C.H., 1990. Anticrack-associated faulting at very high pressure in natural olivine. Nature 348, 720–722.

Griggs, D.T., Baker, D.W., 1969. The origin of deep focus earthquakes. In: Mark, H., Fernback, S. (Eds.), Properties of Matter under Unusual Conditions. Wiley, New York, pp. 23–42.

Griggs, D.T., Handin, J., 1960. Observations on fracture and hypothesis of earthquakes. Geol. Soc. Am. Mem. 79, 347–373.

Hara, T., Kuge, K., Kawakatsu, H., 1996. Determination of the isotropic component of deep focus earthquakes by inversion of normal-mode data. Geophys. J. Int. 127, 515–528.

Hauck, S.A., Phillips, R.J., Hofmeister, A.M., 1999. Variable conductivity: effects on the thermal structure of subducting slabs. Geophys. Res. Lett. 26 (21), 3257–3260.

Hobbs, B.E., Ord, A., 1988. Plastic instabilities: implications for the origin of intermediate and deep focus earthquakes. J. Geophys. Res. 93, 10521–10540.

Houston, H., Williams, Q., 1991. Fast rise times and the physical mechanism of deep earthquakes. Nature 352, 520–522.

Houston, H., Benz, H.M., Vidale, J.E., 1998. Time functions of deep earthquakes from broadband and short-period stacks. J. Geophys. Res. 103, 29895–29914.

Hubbert, M.K., Rubey, W.W., 1959. Role of fluid pressure in mechanics of overthrust faulting. 1. Mechanics of fluid-filled porous solids and its application to overthrust faulting. Geol. Soc. Am. Bull. 70, 115–166.

Ihmle, P.F.I., 1998. On the interpretation of subevents in teleseismic waveforms: the 1994 Bolivia deep earthquake revisited. J. Geophys. Res. 103, 17919–17932.

Iidaka, T., Suetsugu, D., 1992. Seismological evidence for metastable olivine inside a subducting slab. Nature 356, 593–595.

Jiao, W., Silver, P.G., Fei, Y., Prewitt, C.T., 2000. Do deep earthquakes occur on preexisting weak zones? An examination of the Tonga subduction slab. J. Geophys. Res. 105, 28125–28138.

Johnson, T.L., Scholz, C.H., 1976. Dynamic properties of stick-slip friction in rock. J. Geophys. Res. 81, 881–888.

Kagan, Y.Y., Knopoff, L., 1980. Dependence of seismicity on depth. Bull. Seismol. Soc. Am. 70, 1811–1822.

Kanamori, H., Anderson, D.L., 1975. Theoretical basis of some empirical relations in seismology. Bull. Seismol. Soc. Am. 65, 1073–1095.

Kanamori, H., Anderson, D.L., Heaton, T.H., 1998. Frictional melting during faulting. Science 279, 839.

Karato, S.-I., 1997. Phase transformations and rheological properties of mantle minerals. In: Crossleym D.J. (Ed.), Earth's Deep Interior. Gordon and Breach, Amsterdam, pp. 223–272.

Kawakatsu, H., 1996. Observability of the isotropic component of a moment tensor. Geophys. J. Int. 126, 525–544.

Kikuchi, M., 1992. Strain drop and apparent strain for large earthquakes. Tectonophysics 211, 107–113.

Kirby, S.H., 1987. Localized polymorphic phase transformations in high-pressure faults and applications to the physical mechanism of deep earthquakes. J. Geophys. Res. 92, 13789–13800.

Kirby, S.H., Durham, W.B., Stern, L.A., 1991. Mantle phase changes and deep earthquake faulting in subducting lithosphere. Science 252, 216–225.

Kirby, S., Engdahl, E.R., Denlinger, R., 1996a. Intermediate-depth intraslab earthquakes and arc volcanism as physical expressions of crustal and uppermost mantle metamorphism in subducting slabs (overview). In: Bebout, G.E., Scholl, D.W., Kirby, S.H., Platt, J.P. (Eds.), Subduction Top to Bottom. Geophysics Monograph Series, AGU, Washington, DC, pp. 195–214.

Kirby, S.H., Stein, S., Okal, E.A., Rubie, D., 1996b. Deep earthquakes and metastable mantle phase transformations in subducting oceanic lithosphere. Rev. Geophys. 34, 261–306.

Kisslinger, C., 1996. Aftershocks and fault-zone properties. Adv. Geophys. 38, 1–36.

Koper, K.D., Wiens, D.A., 2000. The waveguide effect of metastable olivine in slabs. Geophys. Res. Lett. 27, 573–576.

Koper, K.D., Wiens, D.A., Dorman, L.M., Hildebrand, J.A., Webb, S.C., 1998. Modeling the Tonga slab: can travel time data resolve a metastable olivine wedge? J. Geophys. Res. 103, 30079–30100.

Kuge, K., Kawakatsu, H., 1993. Significance of non-double couple components of deep and intermediate-depth earthquakes: implications from moment tensor inversions of long-period seismic waves. Phys. Earth Planet. Inter. 75, 243–266.

Leith, A., Sharpe, J.A., 1936. Deep focus earthquakes and their geological significance. J. Geol. 44, 877–917.

Marone, C., Liu, M., 1997. Transformation shear instability and the seismogenic zone for deep earthquakes. Geophys. Res. Lett. 24, 1887–1890.

Marton, F.C., Bina, C.R., Stein, S., Rubie, D.C., 1999. Effects of slab mineralogy on subduction rates. Geophys. Res. Lett. 26, 119–122.

McGuire, J.J., Wiens, D.A., Shore, P.J., Bevis, M.G., 1997. The 9 March 1994 Tonga deep earthquake: rupture outside the seismically active slab. J. Geophys. Res. 102, 15163–15182.

McKenzie, D., Brune, J.N., 1972. Melting on fault planes during large earthquakes. Geophys. J. Roy. Astron. Soc. 29, 65–78.

Meade, C., Jeanloz, R., 1991. Deep focus earthquakes and recycling of water into the Earth's mantle. Science 252, 68–72.

Molnar, P., Freedman, D., Shih, J.S.F., 1979. Lengths of intermediate and deep seismic zones and temperatures in downgoing slabs in the mantle. Geophys. J. Roy. Astron. Soc. 56, 41–54.

Myers, S.C., et al., 1995. Implications of spatial and temporal development of the aftershock sequence for the $M_w = 8.3$, 9 June 1994 Bolivian deep earthquake. Geophys. Res. Lett. 22, 2269–2272.

Navrotsky, A., Bose, K., 1995. Thermodynamic stability of hydrous silicates: some observations and implications for water in the Earth, Venus, and Mars. In: Farley, K. (Ed.), Processes of Deep Earth and Planetary Volatiles. American Institute of Physics, New York, pp. 221–228.

Nyffenegger, P., Frohlich, C., 2000. Aftershock occurrence rate decay properties for intermediate and deep earthquake sequences. Geophys. Res. Lett. 27, 1215–1218.

Obata, M., Karato, S., 1995. Ultramafic pseudo-tachylyte from Balmuccia peridotite, Ivrea-Verbania zone, northern Italy. Tectonophysics 242, 313–328.

Ogawa, M., 1987. Shear instability in a visco-elastic material as the cause of deep focus earthquakes. J. Geophys. Res. 92, 13801–13810.

Okal, E.A., Kirby, S.H., 1995. Frequency-moment distribution of deep earthquakes Implications for the seismogenic zone at the bottom of slabs. Phys. Earth Planet. Inter. 92, 169–187.

Okal, E.A., Romanowicz, B.A., 1994. On the variation of *b*-values with earthquake size. Phys. Earth Planet. Inter. 87, 55–76.

Pacheco, J.F., Scholz, C.H., Sykes, L.R., 1992. Changes in frequency-size relationship from small to large earthquakes. Nature 355, 71–73.

Page, R., 1968. Focal depths of aftershocks. J. Geophys. Res. 73, 3897–3903.

Raleigh, C.B., Paterson, M.S., 1965. Experimental deformation of serpentinite and its tectonic significance. J. Geophys. Res. 70, 3965–3985.

Randall, M.J., Knopoff, L., 1970. The mechanism at the focus of deep earthquakes. J. Geophys. Res. 75, 4965–4976.

Rubie, D.C., Ross II, C.R., 1994. Kinetics of the olivine–spinel transformation in subducting lithosphere: experimental constraints and implications for deep slab processes. Phys. Earth Planet. Inter. 86, 223–241.

Rundle, J.B., 1989. Derivation of the complete Gutenberg–Richter magnitude–frequency relation using the principle of scale invariance. J. Geophys. Res. 94, 12337–12342.

Russakoff, D., Ekstrom, G., Tromp, J., 1997. A new analysis of the great 1970 Columbia earthquake and its isotropic component. J. Geophys. Res. 102, 20423–20434.

Schmeling, H., Monz, R., Rubie, D.C., 1999. The influence of olivine metastability on the dynamics of subduction. Earth Planet. Sci. Lett. 165, 55–66.

Silver, P., et al., 1995. Rupture characteristics of the Bolivian deep earthquake of 9 June 1994 and the mechanism of deep focus earthquakes. Science 268, 69–73.

Spray, J.G., 1993. Viscosity determinations of some frictionally generated silicate melts: implications for fault zone rheology at high strain rates. J. Geophys. Res. 98, 8053–8068.

Sung, C.M., Burns, R.G., 1976. Kinetics of high-pressure phase transformations: implications to the evolution of the olivine to spinel transition in the downgoing lithosphere and its consequences on the dynamics of the mantle. Tectonophysics 31, 1–32.

Tajima, F., Kanamori, H., 1985. Global survey of aftershock area expansion patterns. Phys. Earth Planet. Inter. 40, 77–134.

Tatsumi, Y., 1989. Migration of fluid phases and genesis of basalt magmas in subduction zones. J. Geophys. Res. 94, 4697–4707.

Thompson, A.B., 1992. Water in the Earth's upper mantle. Nature 358, 295–302.

Tibi, R., Estabrook, C.H., Bock, G., 1999. The 17 June 1996 Flores Sea and 9 March 1994 Tonga–Fiji earthquakes: source processes and deep earthquake mechanisms. Geophys. J. Int. 138, 625–642.

Tinker, M.A., Beck, S.L., Jiao, W., Wallace, T.C., 1998. Mainshock and aftershock analysis of the 17 June 1996 deep Flores Sea earthquake sequence: implications for the mechanism of deep earthquakes and the tectonics of the Banda Sea. J. Geophys. Res. 103, 9987–10002.

Toksoz, M.N., Sleep, N.H., Smith, A.T., 1973. Evolution of the downgoing lithosphere and the mechanisms of deep focus earthquakes. Geophys. J. Roy. Astron. Soc. 35, 285–310.

Vassiliou, M.S., Kanamori, H., 1982. The energy release in earthquakes. Bull. Seismol. Soc. Am. 72, 371–387.

Vidale, J.E., Houston, H., 1993. The depth dependence of earthquake duration and implications for rupture mechanisms. Nature 365, 45–47.

Wiens, D.A., 1998. Source and aftershock properties of the 1996 Flores Sea deep earthquake. Geophys. Res. Lett. 25, 781–784.

Wiens, D.A., Gilbert, H.J., 1996. Effect of slab temperature on deep earthquake aftershock productivity and magnitude–frequency relations. Nature 384, 153–156.

Wiens, D.A., McGuire, J.J., 1995. The 1994 Bolivia and Tonga events: fundamentally different types of deep earthquakes. Geophys. Res. Lett. 22, 2245–2248.

Wiens, D.A., McGuire, J.J., 2000. Aftershocks of the 9 March 1994 Tonga earthquake: the strongest known deep aftershock sequence. J. Geophys. Res. 105, 19067–19083.

Wiens, D.A., et al., 1994. A deep earthquake aftershock sequence and implications for the rupture mechanism of deep earthquakes. Nature 372, 540–543.

Wiens, D.A., Gilbert, H.J., Hicks, B., Wysession, M.E., Shore, P.J., 1997. Aftershock sequences of moderate-sized intermediate and deep earthquakes in the Tonga subduction zone. Geophys. Res. Lett. 24, 2059–2062.

Willemann, R.J., Frohlich, C., 1987. Spatial patterns of aftershocks of deep focus earthquakes. J. Geophys. Res. 92, 13927–13943.

Wong, T., Ko, S., Olgaard, D.L., 1997. Generation and maintenance of pore pressure excess in a dehydrating system. 2. Theoretical analysis. J. Geophys. Res. 102, 841–852.

Wortel, M.J.R., Vlaar, N.J., 1988. Subduction zone seismicity and the thermo-mechanical evolution of downgoing lithosphere. Pageophysics 128, 625–659.

Wu, L.-R., Chen, W.-P., 1999. Anomalous aftershocks of deep earthquakes in Mariana. Geophys. Res. Lett. 26 (13), 1977–1980.

Yamanaka, Y., Shimazaki, K., 1990. Scaling relationship between the number of aftershocks and the size of the mainshock. J. Phys. Earth 38, 305–324.